Eur. Phys. J. A **17**, 195–212 (2003)
DOI 10.1140/epja/i2003-10007-5

THE EUROPEAN PHYSICAL JOURNAL A

Emission of intermediate-mass fragments in the interaction of ^{16}O with ^{59}Co, ^{93}Nb and ^{197}Au

E. Gadioli[1,a], G.F. Steyn[2], F. Albertini[1], C. Birattari[1], M. Cavinato[1], S.H. Connell[3], A.A. Cowley[4], E. Fabrici[1], S.V. Förtsch[2], E. Gadioli Erba[1], J.J. Lawrie[2], M. Pigni[1], J.P.F. Sellschop[3], and E. Sideras Haddad[3]

[1] Università di Milano and I.N.F.N., Sezione di Milano, Milano, Italy
[2] iThemba Laboratory for Accelerator-Based Sciences, Somerset West 7129, South Africa
[3] Schonland Research Centre, Witwatersrand University, Johannesburg, South Africa
[4] Department of Physics, University of Stellenbosch, Matieland 7602, South Africa

Received: 21 January 2003 / Revised version: 10 March 2003 /
Published online: 5 June 2003 –
Communicated by R.A. Ricci

Abstract. In this paper we study the emission of ^{8}Be$_{gs}$, B and N fragments in the interaction of ^{16}O ions with ^{59}Co, ^{93}Nb and ^{197}Au at incident energies varying from 6 to 25 MeV/nucleon. The spectra of these fragments, as well as those of C fragments studied in a previous paper, are dominated at forward angles by a component originating from break-up of ^{16}O. At the higher incident energies break-up occurs after quite a sizeable projectile energy loss. Another mechanism which dominates at large emission angles, favours the emission of low-energy fragments and is attributed to the coalescence of nucleons during the cascade of nucleon-nucleon interactions by means of which the excited nuclei produced in the primary two-ion interaction thermalize.

PACS. 25.70.Gh Compound nucleus – 25.70.Mn Projectile and target fragmentation

1 Introduction

The emission of clusters, called intermediate-mass fragments (IMF) if they have $Z \geq 3$, is quite a common feature in heavy-ion reactions. Many experimental and theoretical studies have been conducted to explain these emissions in the interaction of many different nuclei at energies varying from a few up to several hundred MeV/nucleon (see for instance [1–13] and references therein). This subject is still widely debated and a generally accepted theory which explains all the observed features is still lacking.

One particular point which needs to be clarified, in our opinion, is whether the IMF are mainly emitted by highly excited nuclei or whether their emission is significant even at rather small excitation energies. In fact, when an equilibrated excited nucleus decays it may be energetically favourable to emit clusters of nucleons instead of the single constituents of these clusters. At low excitation energies (a few tens of MeV) the emission of these clusters is statistically and dynamically suppressed by the reduction of the available phase space and the high Coulomb barrier which opposes their emission. However, with increasing excitation energy to several hundred MeV, the emission of even high-charge IMF is predicted to become comparable to the emission of low-charge ejectiles [1]. If, contrary to these expectations, a quite considerable emission of IMF is observed even at rather low incident energies, it must be attributed to processes different from the statistical emission from equilibrated nuclei or to the structure of the interacting ions. The study of the IMF emission at low incident energies thus seems to be important and may significantly improve our knowledge of both the reaction dynamics and the internal structure of nuclei. Furthermore, it may be simpler to interpret these reactions if one considers the interaction of a light nucleus with a more massive partner —a process of intermediate complexity between that of light-particle–induced reactions of which we have quite a deep understanding [14,15] and the much more complex interaction of two massive nuclei.

For these reasons we have undertaken the study of the emission of $Z \geq 4$ fragments (^{8}Be$_{gs}$, B, C, N) in the interaction of ^{16}O ions with medium-heavy nuclei, (^{59}Co and ^{93}Nb) and, in the case of ^{8}Be$_{gs}$, also a heavy nucleus (^{197}Au) at incident energies varying from 6 to 25 MeV/nucleon. We have observed substantial emission yields of these fragments at all the investigated energies. In this paper, we discuss these results and their possible interpretation. In sect. 2 the experimental set-up is briefly described and the qualitative features of the measured IMF spectra are discussed. In sect. 3 the theories we

[a] e-mail: gadioli@mi.infn.it

propose to reproduce these data are outlined and their predictions compared to the experimental results. Section 4 is devoted to the conclusions.

2 Experimental set-up and qualitative overview of the data

The experiment was performed at the cyclotron facility of the iThemba Laboratory for Accelerator-Based Sciences (formerly known as the National Accelerator Centre) in Somerset West, South Africa. The spectra of $^{8}Be_{gs}$ fragments, at an incident ^{16}O energy of 400 MeV, and of the other heavier fragments at incident energies of 100, 250 and 400 MeV, were measured with two different experimental set-ups. In both cases the incident ^{16}O beam was focused to a spot of about 3 mm in diameter on the ^{59}Co and ^{93}Nb targets, and in the case of the $^{8}Be_{gs}$ measurements also on a ^{197}Au target, the thicknesses of which were of the order of 1 mg/cm^2.

Since the set-up used for the $^{8}Be_{gs}$ measurements had been described in detail in previous papers [16], only a short summary is presented here. The nucleus $^{8}Be_{gs}$ is unbound with a decay time which is so short that it dissociates into two correlated α-particles before reaching the detector. The two α-particles are emitted within a narrow cone around the original $^{8}Be_{gs}$ direction. The opening angle of this cone depends on the $^{8}Be_{gs}$ kinetic energy and varies from about 1.7° to 0.7° for kinetic energies varying from 50 to 300 MeV. This opening angle is substantially larger if ^{8}Be is produced in an excited state. This may be exploited to identify ^{8}Be produced in the ground state. The two α-particles were detected in coincidence using a resonant particle spectrometer (RPS) consisting of a silicon strip detector (SSD) [17–19] in conjunction with a stopping detector. This configuration allows one to obtain ΔE information for both correlated α-particles constituting $^{8}Be_{gs}$, but not the total energy for each of them individually. The total $^{8}Be_{gs}$ energy (*i.e.*, the sum energy of the two α-particles) can, however, be uniquely determined. Two identical RPS telescopes were used in the experiment. The SSDs used have 16 vertical anode strips and 16 horizontal cathode strips each, with a total active area of 50 mm × 50 mm. The effective solid angle (related to the detector efficiency) for $^{8}Be_{gs}$ varied from about 1 msr to 4.2 msr in the energy range of interest, as shown in fig. 1. As shown in this figure, the efficiency is substantially smaller for ^{8}Be fragments produced in the 2^+ first-excited state. Individual strip readouts were provided for all the vertical strips, while the horizontal strips were bussed together to give only two readouts, one for even-numbered strips and one for odd-numbered strips. This required 18 independent channels of electronic instrumentation for each SSD. The strips were 280 μm thick, resulting in a lower energy threshold of about 50 MeV. NaI(Tl) crystals of 3 inch in diameter and 2 inch thickness were used as stopping detectors.

The RPS telescopes were mounted on rotatable arms inside a 1.5 m diameter scattering chamber on opposite sides of the beam axis, in the same reaction plane. A two-fold coincidence was required in hardware between any of the vertical silicon strips in order to generate an event trigger. Conventional ΔE-E particle identification (PID) spectra were generated for each vertical strip in coincidence with the NaI stopping detector. A detailed description of the detector calibration and data analysis is given in ref. [16]. The $^{8}Be_{gs}$ spectra have been measured between 8° and 40°. The absolute cross-sections are accurate within a systematic error of 15%.

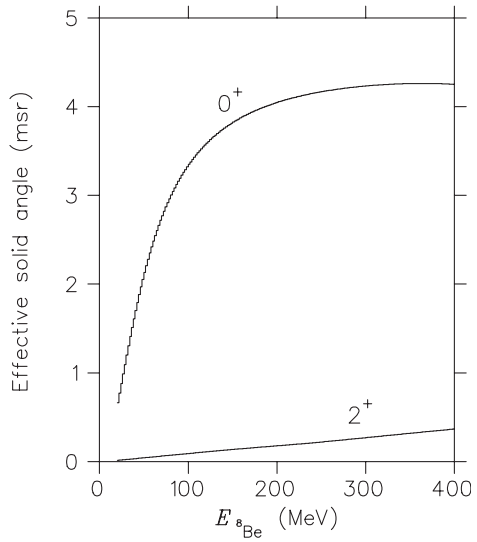

Fig. 1. Effective solid angle for detection of ^{8}Be fragments with the resonant particle spectrometer in our experiment. The solid angle was estimated by Monte Carlo calculations for ^{8}Be in the 0^+ ground state and in the 2^+ first-excited state.

The inclusive spectra of boron, carbon and nitrogen fragments were measured using a different set-up, also consisting of two identical detector telescopes. Each telescope consisted of a 25 μm thick Si surface barrier ΔE detector, followed by a 2 mm thick Si surface barrier stopping (E) detector. Energy calibration of the Si detectors was performed using both the kinematics of elastic scattering and α-particles from a ^{228}Th source. Passive brass collimators were used to define solid angles of 0.7 msr. As in the case of the $^{8}Be_{gs}$ measurements, the beam halo was monitored frequently by comparing the count rate from an empty target frame with that of the rate from the ^{59}Co target at the most forward angles. The standard ΔE-E technique was used for particle identification and allowed a sharp separation of ejectiles of different Z. Unfortunately it did not allow isotope discrimination for each Z. Standard electronics together with an on-line computer were used to write event-by-event data to magnetic tape for subsequent off-line analysis. Electronic dead time was measured and corrected for. It never exceeded 5% at the most forward angles and was generally well below 1% at angles larger than 10°. The spectra were measured at angles between 6° and 50° at 100 MeV, 14° and 50° at 250 MeV and 4° and 50° at 400 MeV. The absolute cross-sections are accurate to within a systematic error of 10%.

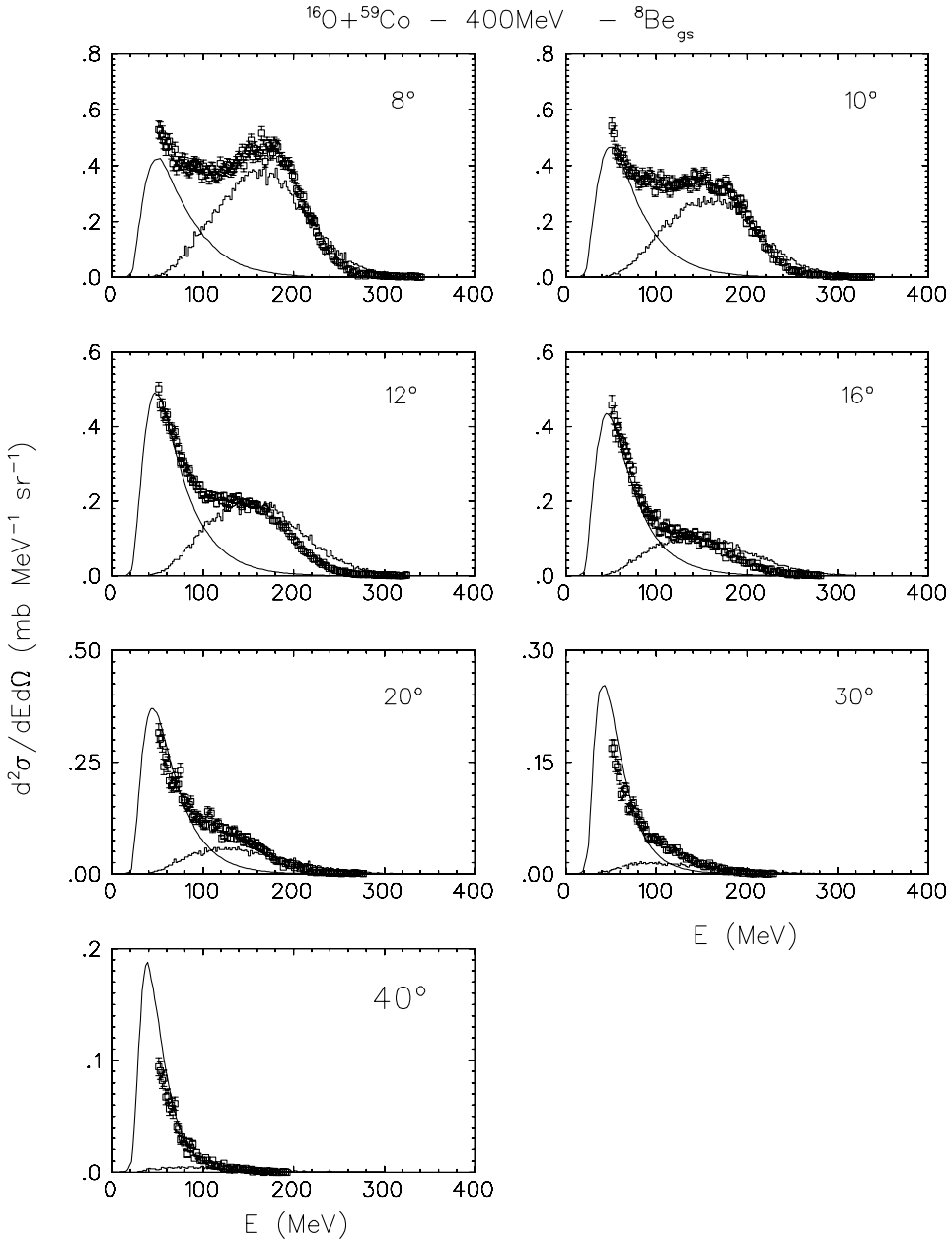

Fig. 2. Spectra of ^{8}Be$_{gs}$ fragments produced in the interaction of ^{16}O with ^{59}Co at an incident energy of 400 MeV. The experimental cross-sections are given by the squares, the theoretical predictions by the full lines (coalescence) and the histograms (break-up).

The spectra of ^{8}Be$_{gs}$, boron and nitrogen are shown at selected angles in figs. 2 to 14. The spectra of carbon have also been measured and have already been presented in a previous paper [20]. A comparison of the results shown in that work with those of the present study is made.

At 100 MeV, the shape of the spectra of the fragments does not change significantly with increasing emission angle and displays quite a broad structure with a maximum at approximately the energy corresponding to the beam velocity, as one expects for projectile break-up. We show in the next section that these spectra are quite reasonably reproduced by the *local plane-wave approximation* (LPWA) suggested by McVoy and Nemes [21]. At 250 and 400 MeV, the spectra are dominated at the most forward angles by a contribution which presumably may still be attributed to the projectile break-up. The yield of this contribution is found to rapidly decrease with increasing emission angle. The average energy of these fragments is smaller than that expected for a *pure* break-up mechanism, *i.e.* in the absence of an initial-state interaction of the projectile before breaking up and/or a final-state interaction of the observed fragment. Also, the width of the energy distribution

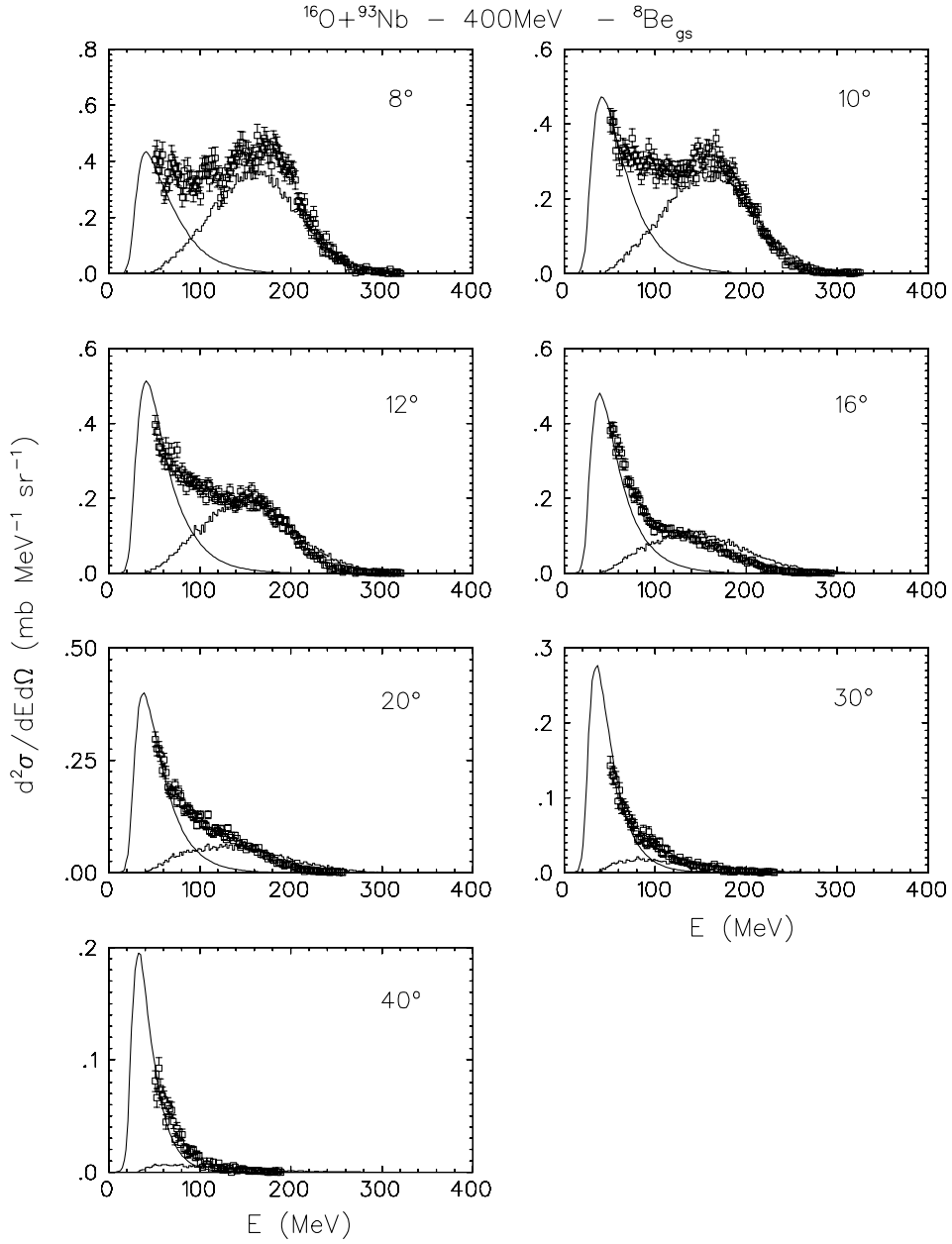

Fig. 3. Spectra of $^{8}Be_{gs}$ fragments produced in the interaction of ^{16}O with ^{93}Nb at an incident energy of 400 MeV. The experimental cross-sections are given by the squares, the theoretical predictions by the full lines (coalescence) and the histograms (break-up).

of these fragments, which, for a pure break-up mechanism should reflect their momentum distribution inside the projectile, is appreciably larger than expected.

A second contribution becomes increasingly important at large angles and dominates beyond about 30°. The yield of this contribution also decreases with increasing emission angle, but much more gently than that of the break-up fragments. It reaches a maximum at a fragment energy about equal to the Coulomb barrier between the observed fragment and the heavy residue. We suggest that these *quasi-evaporated* fragments are produced by nucleon coalescence, before the attainment of thermal equilibrium, after the complete or partial fusion of the projectile and the target [20,22,23].

In the next section we outline the theories which we propose to describe these two contributions and show that they allow a very reasonable reproduction of the energy and angular dependence of the observed IMF spectra.

3 Theoretical analysis

3.1 Fragments originating from break-up of the projectile

The spectra of $^{8}Be_{gs}$ provide an unambiguous information because they correspond to a well-defined fragment in a well-defined energy state. Unfortunately, this is not the

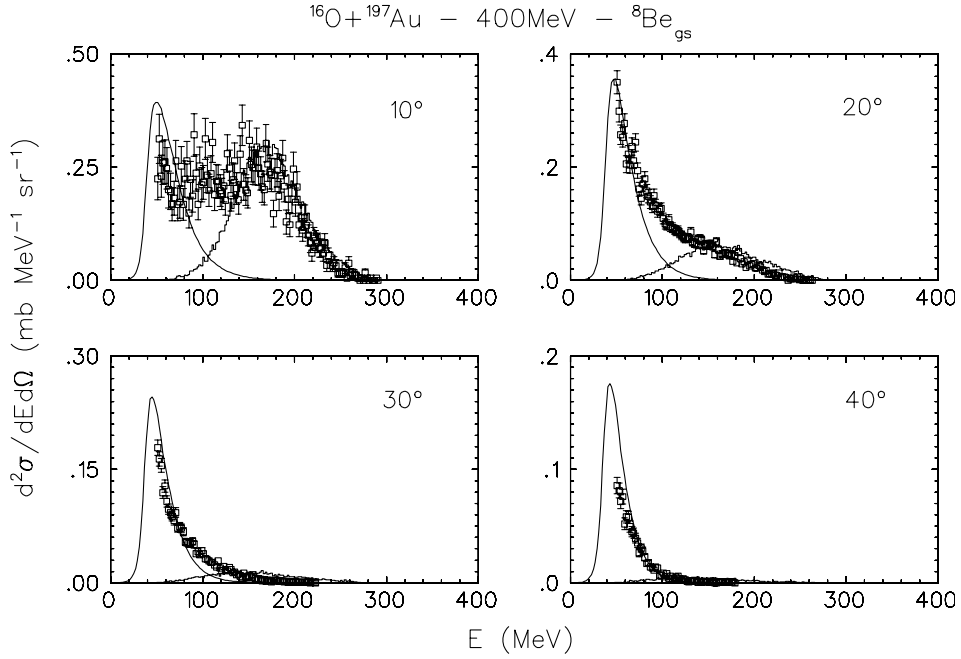

Fig. 4. Spectra of ^{8}Be$_{gs}$ fragments produced in the interaction of ^{16}O with ^{197}Au at an incident energy of 400 MeV. The experimental cross-sections are given by the squares, the theoretical predictions by the full lines (coalescence) and the histograms (break-up).

case for the heavier fragments. In fact, as we remarked before, we could not separate ejectiles of different mass for $Z \geq 5$ and thus in this case we must take into account that more than one isotope may contribute to the break-up and coalescence spectra. According to the theory, the spectra of break-up fragments of different mass have different energy and angular dependences and their analysis may thus suggest the most likely mass of the fragments which one observes.

Previous investigations (see for instance [24]) suggest that the projectile breaks up more easily into fragments of smaller separation energy. As shown in table 1, in the case of boron, the fragment separation energy favours the break-up of ^{16}O into ^{11}B and ^{5}Li. The analysis of the spectra seems indeed to suggest that one observes mostly ^{11}B fragments with a smaller contribution of ^{10}B from ^{16}O break-up into ^{10}B and ^{6}Li. In the case of carbon, the break-up of ^{16}O into a ^{12}C and an α-particle is greatly favoured over other break-up modes. The analysis of the carbon spectra discussed in [20] was indeed made considering only this mode of fragmentation and yielded a very satisfactory reproduction of the data. In the case of nitrogen, even if the separation energy favours the break-up of ^{16}O into a ^{15}N and a proton, the considerable yield of nitrogen observed at rather large angles cannot be explained in this way. This large-angle emission may be explained much more satisfactorily as due to ^{14}N originating from the fragmentation of ^{16}O into a ^{14}N and a deuteron.

As pointed out above, the observed break-up fragments have an average energy which is smaller than expected and have a broader energy distribution. This may be due to either an initial-state interaction of the projectile and/or to a final-state interaction of the observed fragment. The analysis of the spectra of the unstable ^{8}Be$_{gs}$ fragments, both from ^{12}C break-up [16] and from ^{16}O break-up in the present experiment, suggests the prominence of the initial-state interaction. This is because ^{8}Be$_{gs}$ could hardly survive a final-state interaction, which would destroy the strict correlation of the two α-particles into which it dissociates. The analysis of the spectra of the stable ^{12}C fragments in ^{16}O break-up [20] confirmed the validity of this hypothesis which we adopt also for analysing the boron and nitrogen spectra.

Table 1. Separation energies for different binary fragmentations of ^{16}O.

Fragmentation	Separation energy (MeV)
^{15}N + p	12.127
^{14}N + d	20.736
^{13}C + ^{3}He	22.793
^{12}C + ^{4}He	7.162
^{11}C + ^{5}He	26.769
^{11}B + ^{5}Li	25.084
^{10}B + ^{6}Li	30.874
^{8}Be + ^{8}Be	14.620

Our calculations are based on the assumption that projectile break-up, like projectile inelastic scattering, is a peripheral direct reaction occurring in a window of large angular momenta. It has been observed that inelastically

Table 2. Values of the parameters used to evaluate the break-up spectra and of the average energy losses $\overline{\Delta E}$ of ^{16}O ions before breaking up into the various fragments.

^{16}O + ^{59}Co					
E_0 (MeV)	Fragment	C (MeV^{-1})	$E_{\mathrm{l,min}}$ (MeV)	$\overline{\Delta E}$ (MeV)	σ_{bu} (mb)
100	^{10}B	0.1	10	18.5	3
100	^{11}B	0.1	10	18.5	10
100	^{12}C	0.12	16	23.8	147
250	^{10}B	0.015	50	91	16
250	^{11}B	0.015	50	91	50
250	^{12}C	0.02	40	80	181
250	^{14}N	0.012	10	66	88
250	^{15}N	0.08	10	23	108
400	^{8}Be	0.009	55	125	12.5
400	^{10}B	0.009	55	125	27
400	^{11}B	0.009	55	125	81
400	^{12}C	0.02	40	89	288
400	^{14}N	0.012	15	87	108
400	^{15}N	0.08	15	27	108
^{16}O + ^{93}Nb					
E_0 (MeV)	Fragment	C (MeV^{-1})	$E_{\mathrm{l,min}}$ (MeV)	$\overline{\Delta E}$ (MeV)	σ_{bu} (mb)
100	^{10}B	0.1	16	24.8	3
100	^{11}B	0.1	16	24.8	8
250	^{10}B	0.02	50	88	19
250	^{11}B	0.02	50	88	55
250	^{12}C	0.02	45	87	150
250	^{14}N	0.015	25	76	45
250	^{15}N	0.08	30	42	63
400	^{8}Be	0.01	75	148	12.5
400	^{10}B	0.02	70	117	30
400	^{11}B	0.015	70	129	90
400	^{12}C	0.02	45	94	339
400	^{14}N	0.015	40	101	63
400	^{15}N	0.08	40	53	105

scattered ions may lose a considerable fraction of their energy [25–27] and this most presumably happens also before break-up. We assume that the probability of the projectile surviving a break-up or a mass transfer reaction decreases exponentially with increasing projectile energy loss. This is similar to how the inelastic-scattering cross-section averaged over the emission energy decreases exponentially with increasing excitation energy of the target nucleus. Following this assumption the spectra of break-up fragments are evaluated by folding the LPWA cross-section with an exponential survival probability [16,20]. Furthermore, assuming that break-up may occur only after a minimal energy loss $E_{\mathrm{l,min}}$, the double differential cross-section of a fragment emitted at the angle θ with energy E' in the break-up of a projectile with incident energy E_0 is given by

$$\frac{\mathrm{d}^2\sigma}{\mathrm{d}E'\mathrm{d}\Omega}(E_0,E',\theta)=\sigma_{\mathrm{bu}}\frac{\int_{E_{\mathrm{l,min}}}^{E_0}P(E_{\mathrm{l}})S(E,E',\theta)\mathrm{d}E_{\mathrm{l}}}{\int_{E_{\mathrm{l,min}}}^{E_0}P(E_{\mathrm{l}})\mathrm{d}E_{\mathrm{l}}}, \tag{1}$$

where σ_{bu} is the angle and energy integrated break-up cross-section and E_{l} is the energy lost by the projectile before break-up.

$$P(E_{\mathrm{l}})=\exp[-C(E_{\mathrm{l}}-E_{\mathrm{l,min}})] \tag{2}$$

is the survival probability and

$$S(E,E',\theta)=\mathrm{d}^2\sigma^S(E,E',\theta)/\mathrm{d}E'\mathrm{d}\Omega \tag{3}$$

is the cross-section for producing a fragment of energy E' at the angle θ in the break-up of a projectile of energy $E=E_0-E_{\mathrm{l}}$. In the LPWA [21,28]

$$\frac{\mathrm{d}^2\sigma^S(E,E',\theta)}{\mathrm{d}E'\mathrm{d}\Omega}\propto P'\ \ P''\ \ |\psi(\mathbf{p})|^2, \tag{4}$$

where

$$\psi(\mathbf{p})=\frac{1}{(2\pi\hbar)^{3/2}}\int\psi(r)\exp\Big[-\frac{i}{\hbar}(\mathbf{p}\cdot\mathbf{r})\Big]\mathrm{d}\mathbf{r} \tag{5}$$

is the Fourier transform of the wave function describing the relative motion of the fragment within the projectile. The internal momentum of the fragment is given by

$$\mathbf{p} = \mathbf{P'} - (m_{\rm f}/m_{\rm P})\mathbf{P}, \tag{6}$$

where $\mathbf{P}$ is the projectile's momentum when it breaks up (that is, after the energy loss) and $\mathbf{P'}$ is the momentum of the observed fragment just after break-up (which differs from the observed momentum since, after being produced, the fragment is boosted by the Coulomb repulsion). P'' is the modulus of the momentum of the unobserved fragment and $m_{\rm P}$ and $m_{\rm f}$ are, respectively, the masses of the projectile and the observed fragment. The wave function for the relative motion of each couple of fragments, within ^{16}O, with the lowest angular momentum compatible with conservation of spin and parity, is for $L = 0$, the most common occurrence, that corresponding to a square-well interaction potential. The depth and width of this potential well are fitted to give the correct fragment separation energy. This approximation gives an easily handled analytical expression for the Fourier transform [29]. For $L \geq 1$ we evaluated the relative motion wave function, in the cluster approximation, using a Saxon-Woods potential. The values of the parameters C, $E_{\rm l,min}$ and $\sigma_{\rm bu}$ which we use to evaluate the spectra of fragments produced by projectile break-up at the different bombarding energies, are obtained by a best fit of the experimental spectra and are given in table 2 for the interaction of ^{16}O with ^{59}Co and ^{93}Nb. The table also reports the values found for these quantities in the analysis of the ^{12}C spectra [20].

The most significant quantity is $\overline{\Delta E}$, the average kinetic energy lost before break-up. At 100 MeV incident energy it is essentially that part of the incident energy which transforms into Coulomb potential energy and is in part given back to the observed fragment when it is boosted by the Coulomb repulsion after break-up. At 250 and 400 MeV $\overline{\Delta E}$ is considerably greater than any reasonable value of the Coulomb repulsion of the target and this leads us to assume that part of projectile's energy has been transformed into excitation energy. The kinetic energy loss $\overline{\Delta E}$ was found to be about 140 MeV for ^{16}O breaking into two ^{8}Be$_{\rm gs}$ at 400 MeV.

Even if we do not provide a dynamical description of the process by which the projectile loses energy before breaking up, it is conceivable that the energy loss occurs when the two ions come into contact. After break-up both fragments may be emitted without any further significant interaction, or the participant fragment may to a larger or lesser extent violently interact or even fuse with the target nucleus. The observation of only the spectator fragments cannot provide a unique explanation of the processes which occur. However, together with complementary studies, *e.g.*, the comparison of the experimental and calculated cross-sections for residue production in the interaction of ^{12}C and ^{16}O with nuclei at incident energies comparable to the ones which we consider in this paper, and the comparison of the measured and calculated recoil properties of these residues (ranges, angular distributions, and doppler shifts and broadening of emission γ-lines) [30–32], we think that enough evidence exists to conclude that in a large fraction of cases the projectile break-up is followed by the fusion of the participant fragment with the target nucleus. This seems to be substantiated by the results summarized in table 2. There is, in fact, some indication that $\overline{\Delta E}$ decreases with the increasing mass of the observed fragment. If the projectile break-up is in most cases accompanied by the fusion with the target nucleus of the participant fragment, it is reasonable to assume that the angular momentum of the projectile increases with decreasing mass of the fragment which fuses with the target [33,34]. This presumably leads to a corresponding decrease of its energy loss.

As mentioned at the beginning of this section, the analysis of the spectra of ^{8}Be$_{\rm gs}$ fragments is particularly significant because they are not contaminated by the presence of other beryllium isotopes and correspond to fragments in a well-defined state. As shown in figs. 2 to 4, the calculated break-up contributions to the measured spectra at 400 MeV (histograms) is satisfactorily reproduced.

The spectra of B fragments are calculated assuming that, at all energies, ^{16}O fragmentation into ^{11}B and ^{5}Li is about three times more likely than fragmentation into ^{10}B and ^{6}Li. These spectra are given by the histograms in figs. 5 to 10. At 100 MeV the break-up is the only contributing mechanism. At 250 MeV, where the lowest observation angle was 14°, the spectral shape may only be reproduced at all angles by also including the coalescence contribution. Nevertheless, in the more forward direction, where the break-up contribution dominates, our calculated break-up spectra seem to fit the data nicely. At 400 MeV, where the minimum observation angle was as small as 4°, the break-up part is much more discernible and the agreement with the calculation is very encouraging.

To analyse the spectra of the nitrogen fragments shown in figs. 11 to 14, we first considered the fragmentation of ^{16}O into a ^{15}N and a proton. This was found unsatisfactory for two reasons: The first is that this assumption does not allow one to reproduce the quite significant nitrogen emission between 20° and 30°. The second is that even at smaller emission angles, the calculated ^{15}N spectra do not reproduce the measured ones satisfactorily. The measured spectra, below about 12°, are harder than the calculated ones. This seems to agree with the results of much more sophisticated calculations of the spectra of heavy fragments produced in neutron transfer reactions [35], which is a rather similar process. These calculations show that these spectra cannot be only explained as due to the break-up of the projectile into a neutron and a heavy fragment and the subsequent transfer of the rather energetic neutron to a highly excited redidue's state. The small-angle spectra are much more satisfactorily reproduced by a mechanism favouring the transfer of a neutron to a residue's bound state, suggesting that, in this case, the interaction between the projectile and the target is dominated by structure effects. The quite complex calculations needed to evaluate the spectra of heavy fragments produced in proton transfer reactions, with the same mechanism, have

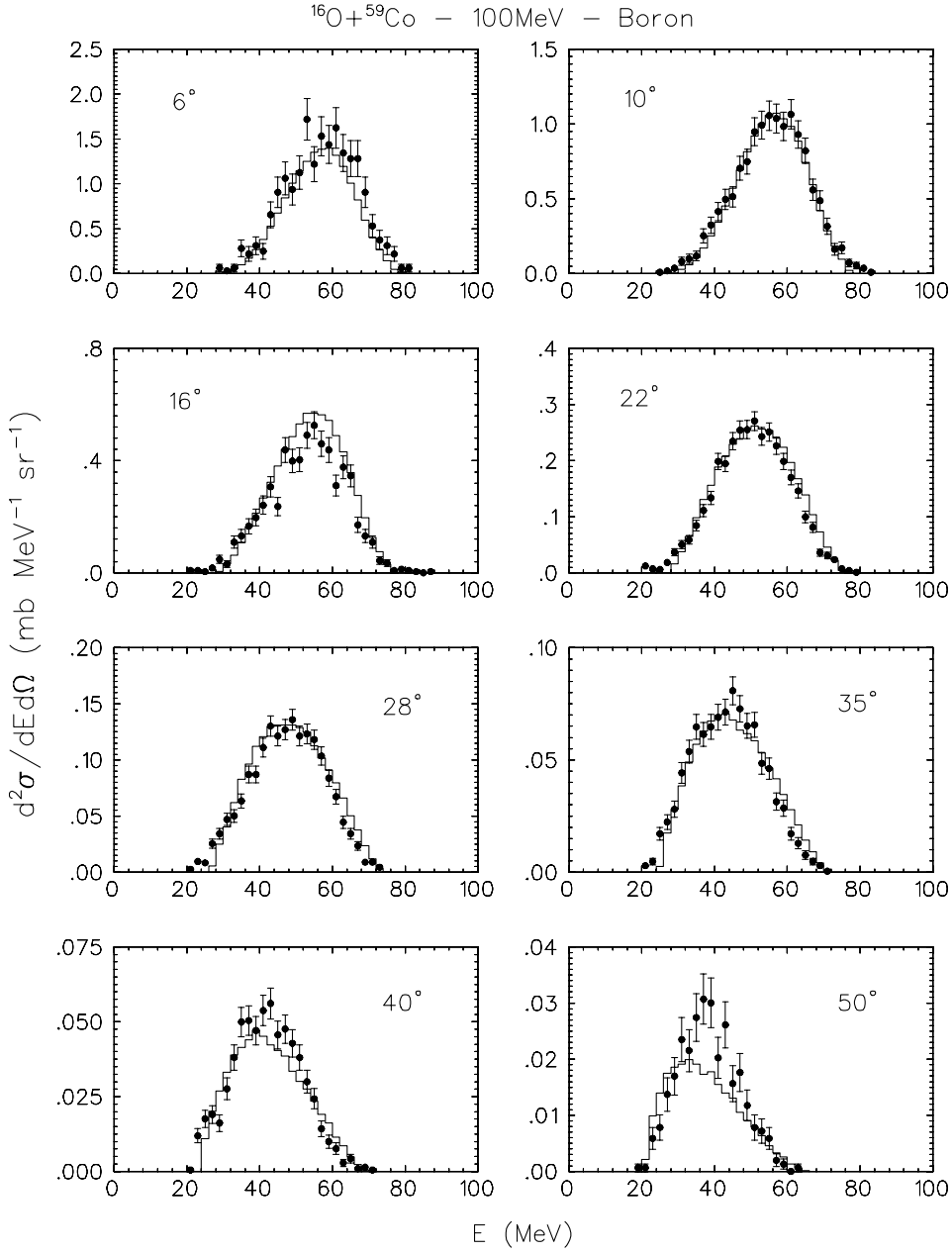

Fig. 5. Spectra of boron fragments produced in the interaction of ^{16}O with ^{59}Co at an incident energy of 100 MeV. The experimental cross-sections are given by the black circles, the theoretical break-up spectra by the histograms.

not been done yet. So, for the time being, we cannot include this contribution in the calculated nitrogen spectra and thus the cross-sections for production of ^{15}N given in table 2 certainly underestimate the actual ones. The observed yield of nitrogen at larger angles is quite nicely reproduced by assuming it to be due to ^{14}N fragments produced by break-up of ^{16}O into a ^{14}N and a deuteron.

In general, the agreement of experimental and calculated spectra is encouraging, considering the relative simplicity of our calculations. Nevertheless, one may see that especially at the higher incident energies, the calculation underestimates the yield of break-up fragments at the largest emission angles. This is likely due to the use of the folding function of eq. (2) which depends only on energy. It is conceivable that fragments produced in the break-up of incident ions which have been appreciably deflected from their initial trajectory as a consequence of the initial inelastic-scattering interaction, may contribute significantly at the largest emission angles. To account for this possibility, the parameter C in eq. (2) should display an angular dependence which we have neglected. The inclusion of such a dependence, which is actually under study, should increase the large-angle yield of break-up fragments quite substantially, improving the agreement of the experimental and the calculated spectra.

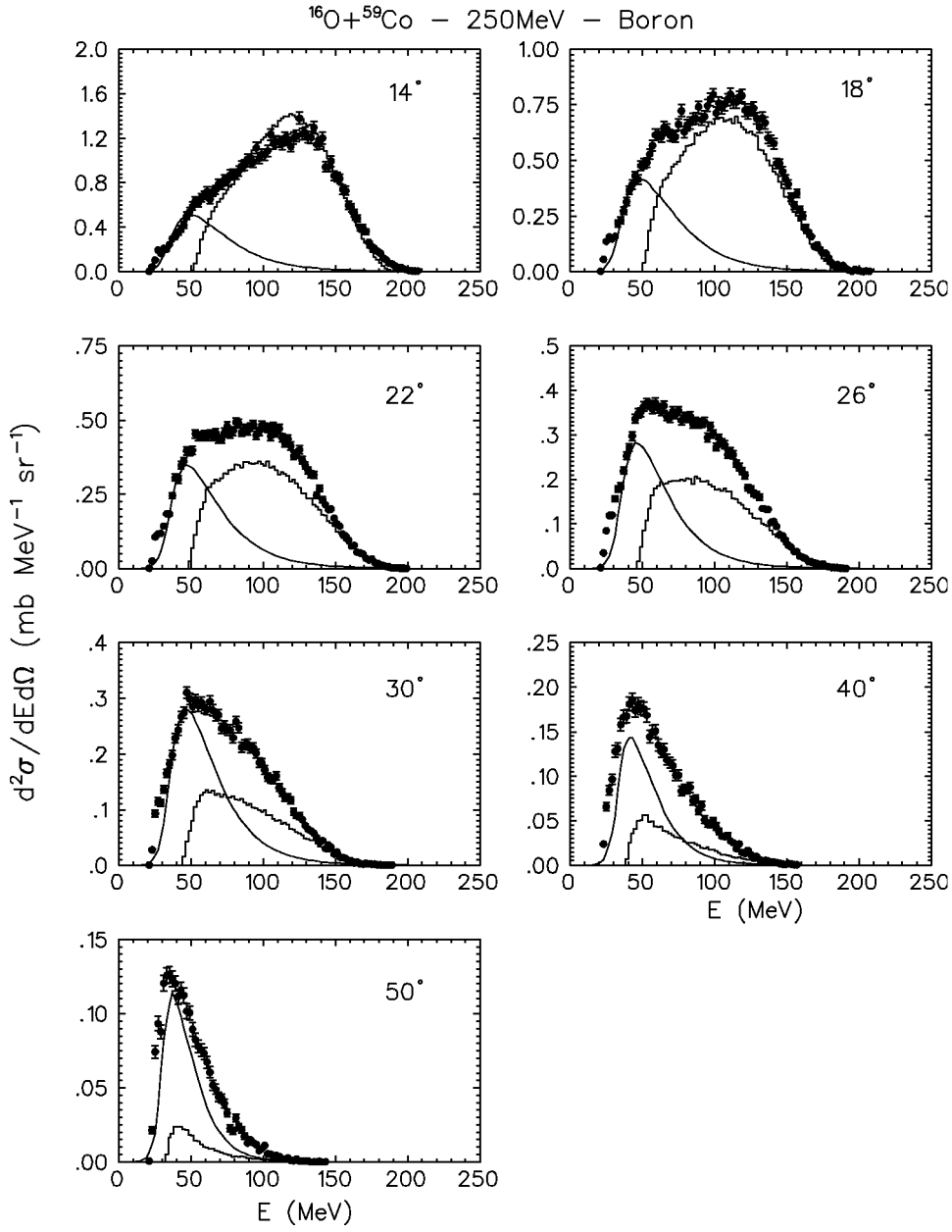

Fig. 6. Spectra of boron fragments produced in the interaction of ^{16}O with ^{59}Co at an incident energy of 250 MeV. The experimental cross-sections are given by the black circles, the theoretical predictions by the full lines (coalescence) and the histograms (break-up).

3.2 Fragments produced by nucleon coalescence

The fusion of the projectile with the target nucleus or the fusion of a participant fragment with the target nucleus after projectile break-up, creates a non-equilibrated excited nucleus. Statistical equilibrium is subsequently reached through a cascade of nucleon-nucleon (N-N) interactions during which nucleons or clusters of nucleons may be emitted with higher emission energies than expected from evaporation by an equilibrated system, and in the case of clusters, a much higher yield.

We simulate the cascade of nucleon-nucleon interactions by means of the Boltzmann Master Equation (BME) theory [36,37] originally proposed by Harp, Miller and Berne [38] and extended by some of the present authors to include the emission of clusters created by nucleon coalescence [22,23].

In this theory, to evaluate the spectra of the particles which are emitted, one needs to know the momentum distribution of the nucleons of the excited nucleus, given by the occupation probabilities of bins in which the momentum space is divided. To evaluate inclusive particle spectra one may exploit the azimuthal symmetry with respect to

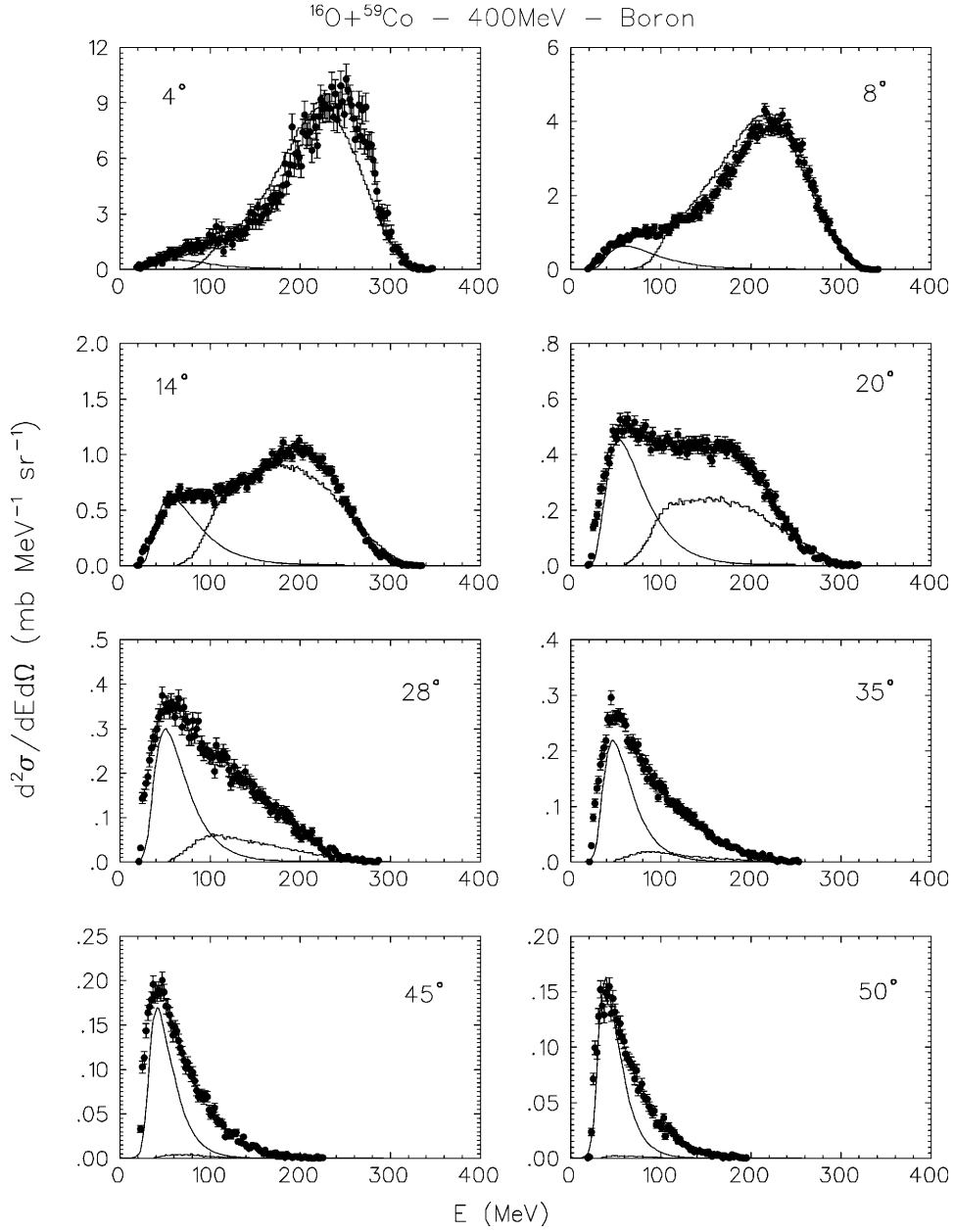

Fig. 7. Spectra of boron fragments produced in the interaction of ^{16}O with ^{59}Co at an incident energy of 400 MeV. The experimental cross-sections are given by the black circles, the theoretical predictions by the full lines (coalescence) and the histograms (break-up).

beam direction and use as variables p^2, the square of the nucleon's momentum, and p_z, its component along the beam axis. The bins may thus be characterized by constant values of Δp^2 (or $\Delta\epsilon$) and Δp_z. In the following the bin indices label momentum space intervals with volume $V_p = \Delta\epsilon\Delta p_z$ centered around given values of the energy ϵ_i, and $(p_z)_i$. The bin occupation probabilities $n_i(\epsilon, \theta, t)$ are a function of time, nucleon energy and θ, the angle between the nucleon momentum and the projectile direction. Initially, the momentum distribution of the nucleons of the excited nucleus is given by a set of occupation probabilities $n_i(\epsilon, \theta, t = 0)$. The occupation probabilities at a subsequent time t are evaluated by integrating the set of Boltzmann Master Equations (BME) given below for protons [36,37]:

$$\begin{aligned}\frac{\mathrm{d}(n_i g_i)^\pi}{\mathrm{d}t} = &\sum_{jlm}[\omega^{\pi\pi}_{lm\to ij} g^\pi_l n^\pi_l g^\pi_m n^\pi_m (1-n^\pi_i)(1-n^\pi_j) \\ &-\omega^{\pi\pi}_{ij\to lm} g^\pi_i n^\pi_i g^\pi_j n^\pi_j (1-n^\pi_l)(1-n^\pi_m)] \\ &+\sum_{jlm}[\omega^{\pi\nu}_{lm\to ij} g^\pi_l n^\pi_l g^\nu_m n^\nu_m (1-n^\pi_i)(1-n^\nu_j) \\ &-\omega^{\pi\nu}_{ij\to lm} g^\pi_i n^\pi_i g^\nu_j n^\nu_j (1-n^\pi_l)(1-n^\nu_m)] \\ &-n^\pi_i g^\pi_i \omega^\pi_{i\to i'} g^\pi_{i'} \delta(\epsilon^\pi_i - \epsilon^\pi_\mathrm{F} - B^\pi_i - \epsilon^\pi_{i'}) - \frac{\mathrm{d}D^\pi_i}{\mathrm{d}t} \end{aligned} \quad (7)$$

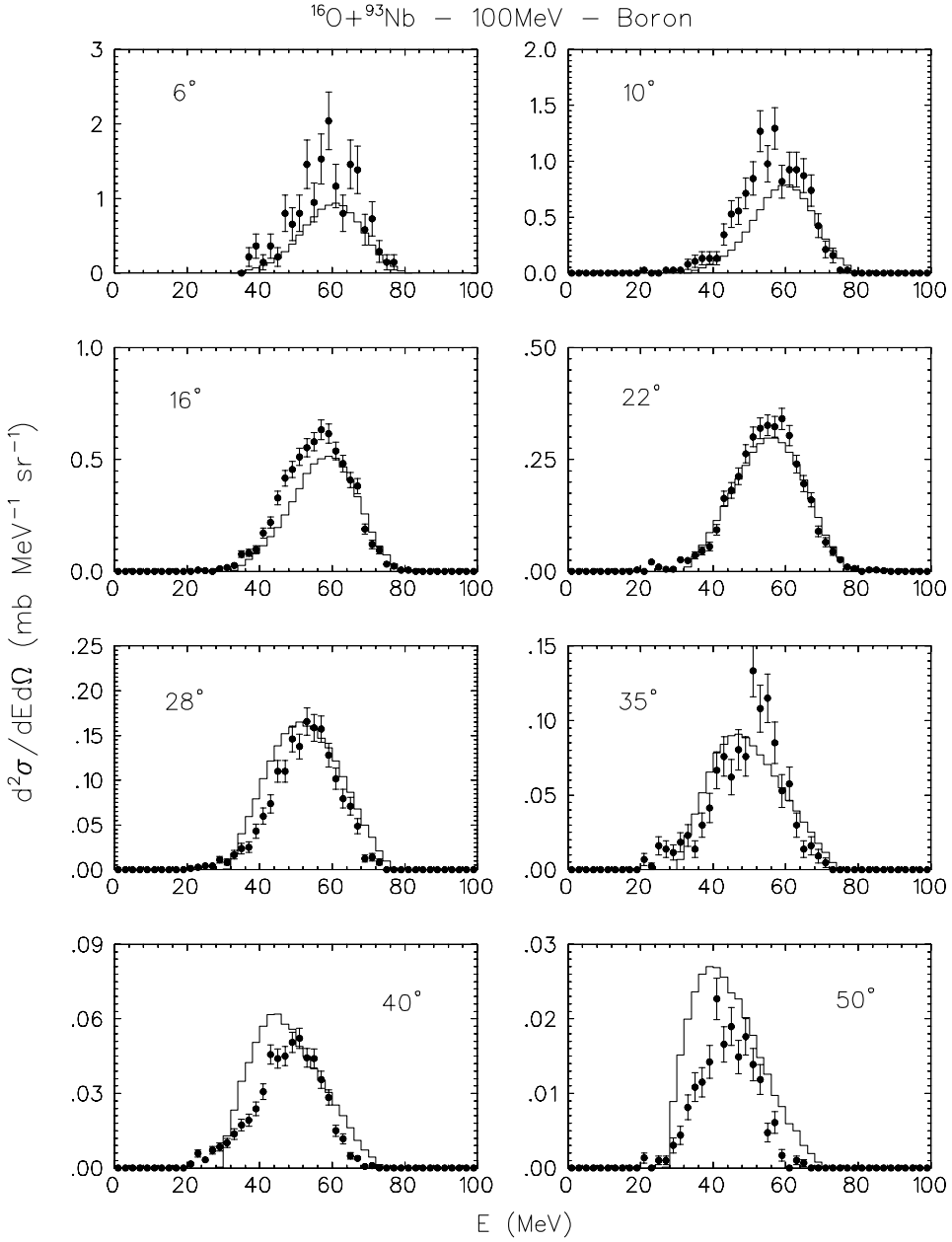

Fig. 8. Spectra of boron fragments produced in the interaction of ^{16}O with ^{93}Nb at an incident energy of 100 MeV. The experimental cross-sections are given by the black circles, the theoretical break-up spectra by the histograms.

(π and ν indicate the protons and the neutrons). An analogous set of equations holds for the neutrons.

The quantities g_i are the total number of states in bin i, $\omega_{ij\to lm}$, $\omega^{\pi}_{i\to i'}$ and $\mathrm{d}D^{\pi}_i/\mathrm{d}t$, whose expressions may be found in [36], are, respectively, the internal transition decay rates (the probability per unit time of a two-nucleon interaction), the decay rates for emission of single protons of the i-th bin into the continuum, and a depletion term which accounts for the emission of protons of the i-th bin which are part of a cluster. These aggregates may be created, during the cascade of N-N interactions, by coalescence of nucleons with momenta within a sphere of radius $p_{\mathrm{c,F}}$ in momentum space. If not immediately emitted they dissolve into their constituents and thus do not contribute to the thermalization interactions inside the nuclear matter. The cluster's multiplicity spectrum is given by

$$\frac{\mathrm{d}^2 M_{\mathrm{c}}(E'_{\mathrm{c}},\theta_{\mathrm{c}})}{\mathrm{d}E'_{\mathrm{c}}\mathrm{d}\Omega} = \frac{R_{\mathrm{c}}}{2\pi\sin\theta_{\mathrm{c}}}\int N_{\mathrm{c}}(E_{\mathrm{c}},\theta_{\mathrm{c}},t)\frac{\sigma_{\mathrm{inv,c}}v_{\mathrm{c}}}{V}\rho_{\mathrm{c}}(E'_{\mathrm{c}},\theta_{\mathrm{c}})\mathrm{d}t\,, \quad (8)$$

where E_{c} and E'_{c} are, respectively, the cluster's energy inside and outside the nucleus and $N_{\mathrm{c}}(E,\theta_{\mathrm{c}},t)$, which represents the probability that the momenta of $(Z_{\mathrm{c}}+N_{\mathrm{c}})$ nucleons are correlated in such a way to move together as a

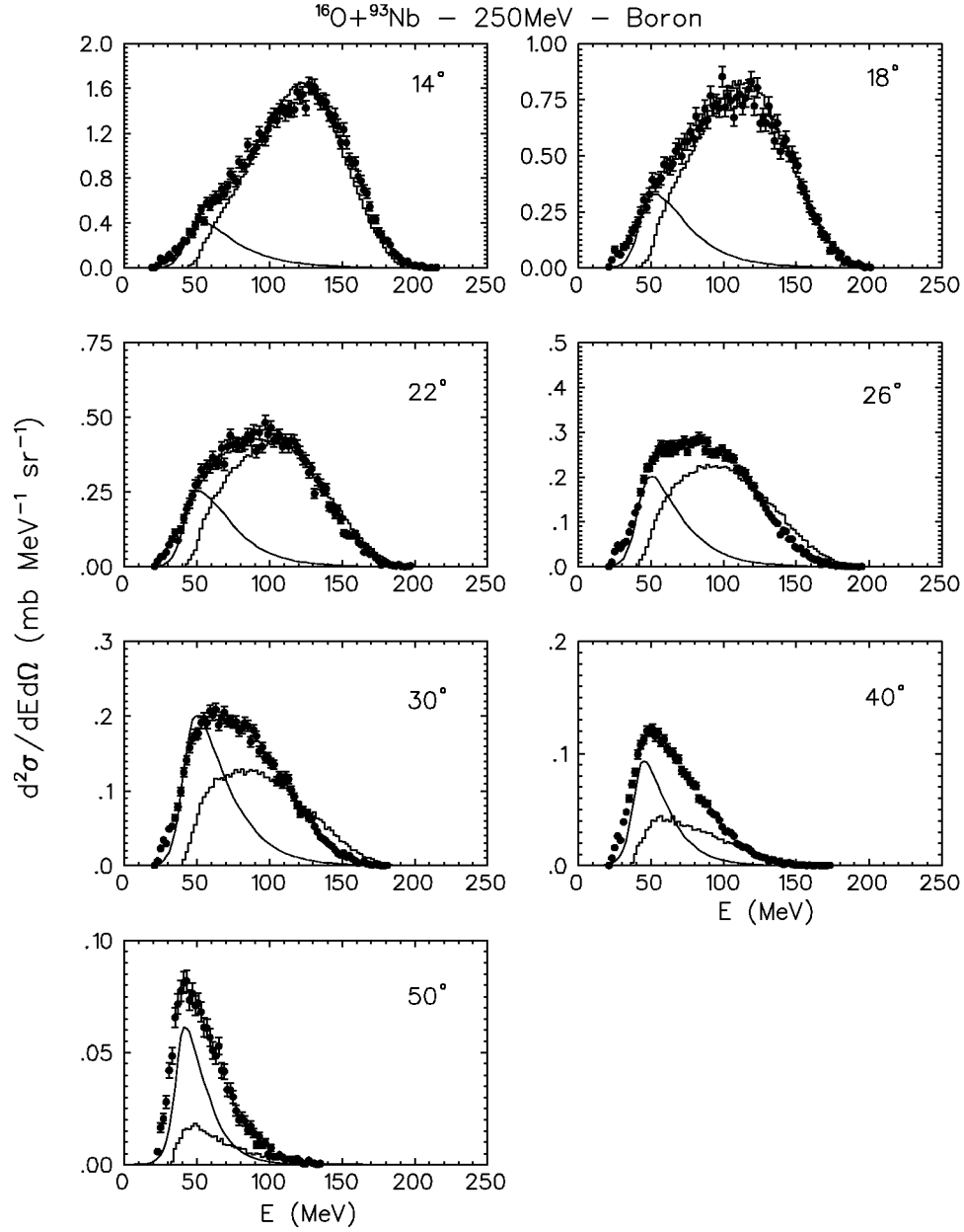

Fig. 9. Spectra of boron fragments produced in the interaction of ^{16}O with ^{93}Nb at an incident energy of 250 MeV. The experimental cross-sections are given by the black circles, the theoretical predictions by the full lines (coalescence) and the histograms (break-up).

cluster with centre-of-mass energy $E_{\rm c}$ inside the composite nucleus, is a function of the state occupation probabilities $n_i(\epsilon,\theta,t)$ of the nucleons constituting the cluster. For a cluster of $Z_{\rm c}$ protons and $N_{\rm c}$ neutrons, it is given by [22,23]

$$N_{\rm c}(E,\theta_{\rm c},t) = \prod_i \left(n_i^{\pi}(\epsilon,\theta,t)\right)^{P_i(E_{\rm c},\theta_{\rm c})Z_{\rm c}} \cdot \prod_i \left(n_i^{\nu}(\epsilon,\theta,t)\right)^{P_i(E_{\rm c},\theta_{\rm c})N_{\rm c}}, \quad (9)$$

where the index i runs over all the bins in which the momenta of the protons and the neutrons of the cluster may be, and $P_i(E_{\rm c},\theta_{\rm c})$ is the fraction of bin i within the cluster Fermi sphere of radius $p_{\rm c,F}$. $\sigma_{\rm inv,c}$ is the inverse process cross-section, $v_{\rm c}$ the relative velocity between the emitted cluster and the residual nucleus, and V the laboratory volume which cancels with an equal term appearing in the expression of $\rho_{\rm c}(E'_{\rm c},\theta_{\rm c})$, the density of cluster states in the continuum. $R_{\rm c}$ is a numerical factor (≤ 1) which accounts for the probability that the nucleons constituting the cluster be confined within the cluster volume in co-ordinate space and that the cluster once formed be emitted before dissolving again into its constituents.

As shown before, the contribution due to nucleon coalescence was observed only at the two higher energies (250 and 400 MeV). This is because at 100 MeV, where

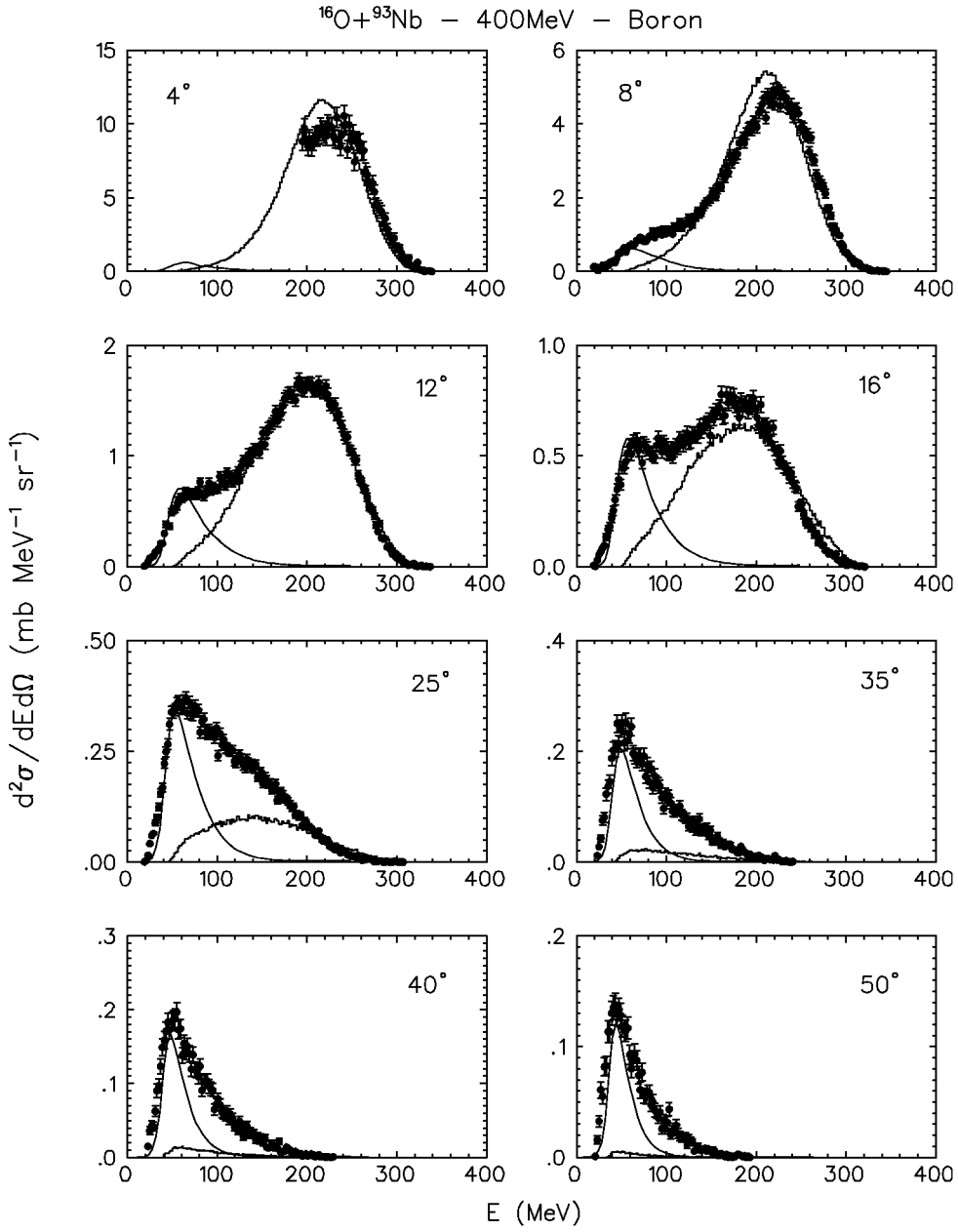

Fig. 10. Spectra of boron fragments produced in the interaction of ^{16}O with ^{93}Nb at an incident energy of 400 MeV. The experimental cross-sections are given by the black circles, the theoretical predictions by the full lines (coalescence) and the histograms (break-up).

complete fusion is dominant, the overlap of the two ions, slowed by their Coulomb repulsion, takes so long that the orderly energy of the projectile's nucleons transforms into thermal energy when they still form a dinuclear system and a large part of the Coulomb potential energy is not yet re-transformed into nucleon kinetic energy [39]. This greatly hinders the emission of pre-equilibrium particles. At higher incident energy, the two ions overlap much faster and their nucleons may even increase their energy when they fall in the common potential well because the composite nucleus Fermi energy is greater than those of the projectile and the target [40].

Several boron and nitrogen isotopes (which are not separated in the experiment) may contribute to the observed coalescence spectra. We have considered all the isotopes which, once emitted, may reach the detector before dissociating into smaller-mass fragments: for boron those with mass from 8 to 14 (except ^{9}B, which immediately dissociates into two alphas and a proton) and for nitrogen those with mass between 12 and 18. The relative yields of the isotopes do not only depend on their mass numbers A but also on their mass excess (which increases or reduces their emission energies), spin and Fermi energy

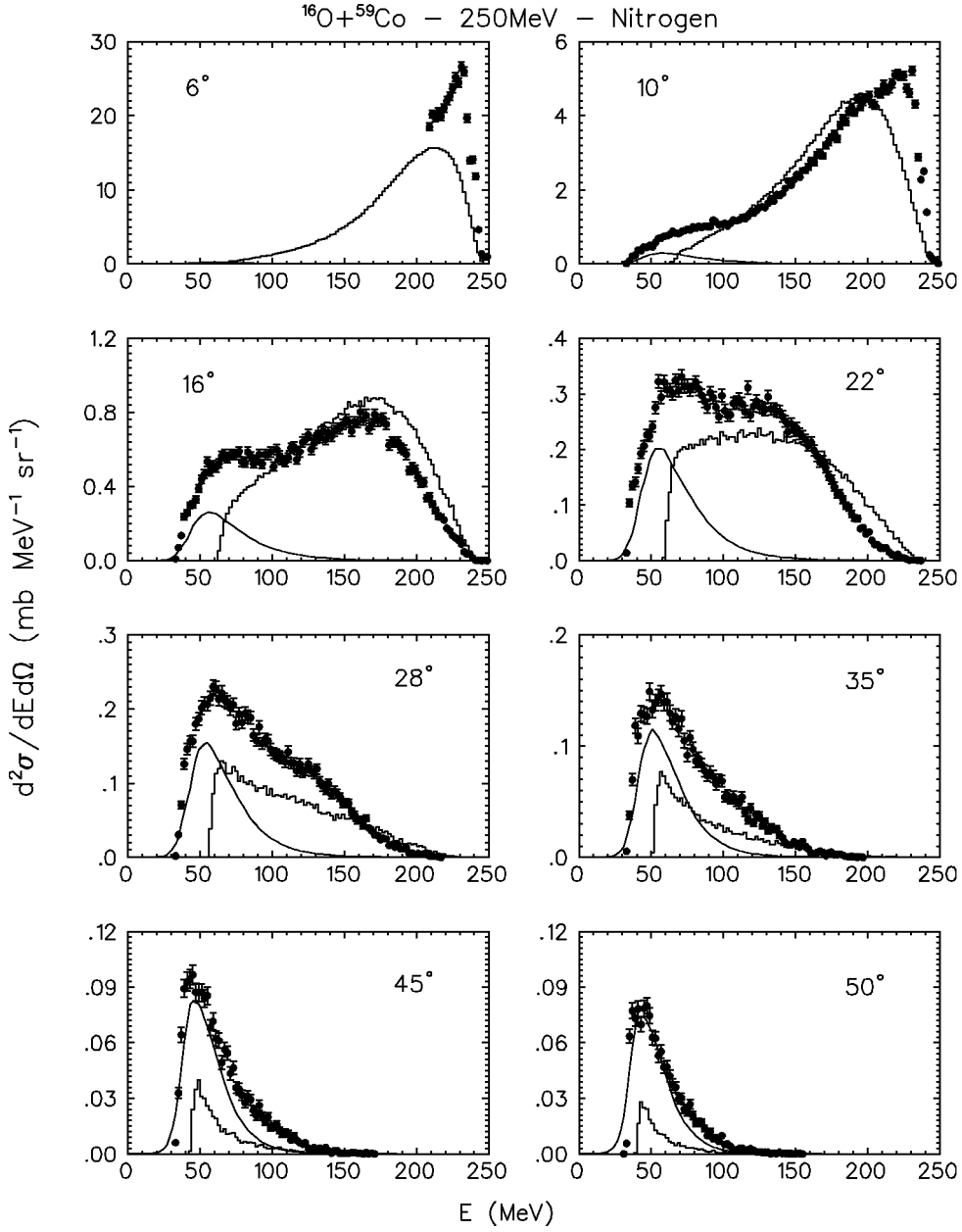

Fig. 11. Spectra of nitrogen fragments produced in the interaction of ^{16}O with ^{59}Co at an incident energy of 250 MeV. The experimental cross-sections are given by the black circles, the theoretical predictions by the full lines (coalescence) and the histograms (break-up).

$E_{\mathrm{c,F}} = p^2_{\mathrm{c,F}}/2m$. Thus, even if one could naively think that the emission of the lower-mass isotopes should be favoured in a process ruled by chance, such as for coalescence, this does not necessarily happen. As in [20,40], we take for the cluster Fermi energies the values predicted by the liquid-drop model with a surface energy correction

$$\epsilon_{\mathrm{F}} = \frac{1}{A}[Z\epsilon^Z_{\mathrm{F}} + N\epsilon^N_{\mathrm{F}}] \tag{10}$$

with

$$\epsilon^Z_{\mathrm{F}} = E_{\mathrm{F}}\frac{2Z^{\frac{2}{3}}}{A}(1 - 0.387A^{-\frac{1}{3}})^2 \tag{11a}$$

and

$$\epsilon^N_{\mathrm{F}} = E_{\mathrm{F}}\frac{2N^{\frac{2}{3}}}{A}(1 - 0.387A^{-\frac{1}{3}})^2. \tag{11b}$$

As in [20], for the nuclear-matter Fermi energy E_{F} we take the value $E_{\mathrm{F}} = 43.5$ MeV, a rather large value which, in the case of boron and nitrogen fragments, may be an effective way of simulating the emission of slightly excited clusters. The boron isotope which, according to our calculations, is emitted with the highest probability, is ^{10}B. The nitrogen fragments produced with higher yield are ^{14}N and ^{13}N.

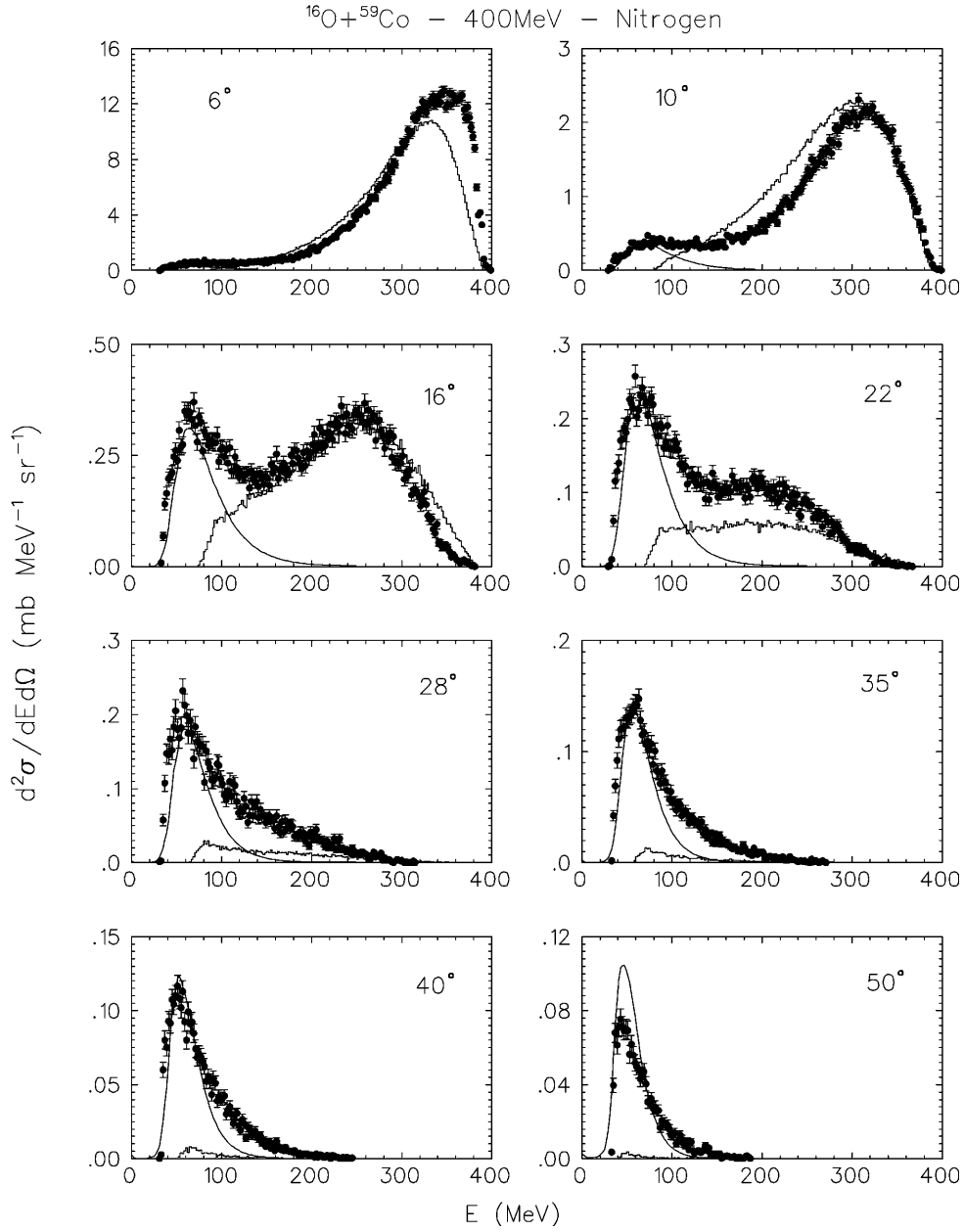

Fig. 12. Spectra of nitrogen fragments produced in the interaction of ^{16}O with ^{59}Co at an incident energy of 400 MeV. The experimental cross-sections are given by the black circles, the theoretical predictions by the full lines (coalescence) and the histograms (break-up).

The coalescence fragments may be produced with comparable yield both in the complete fusion of oxygen with the target nucleus and in the partial fusion of a ^{12}C fragment. The cross-sections for complete and partial fusion which we used in these calculations are, for ^{59}Co and ^{93}Nb, those used previously in [20]. For ^{197}Au we used for σ_{cf} the value predicted by [41] and for σ_C a value tentatively extrapolated from those adopted for ^{59}Co and ^{93}Nb, which were estimated from the values of the reaction and complete fusion cross-sections [41] and the measured cross-section of break-up fragments. These values are given in table 3.

At the lowest energies, in the case of ^{59}Co and ^{93}Nb, the calculations accurately reproduce the measured spectra only if one assumes that the coalescence fragments are emitted by deformed composite nuclei (which we take, for simplicity, to have the shape of rotational ellipsoids with symmetry axis in the beam direction) thus sensing an angle-dependent Coulomb barrier. The ratio of the minor to the major axis which gave the best reproduction, was found to be about 0.6 for nuclei created in the complete or partial fusion of ^{16}O with ^{59}Co and 0.9 for those created in the complete or partial fusion of ^{16}O with ^{93}Nb. This does not seem to be unreasonable considering the remarkably

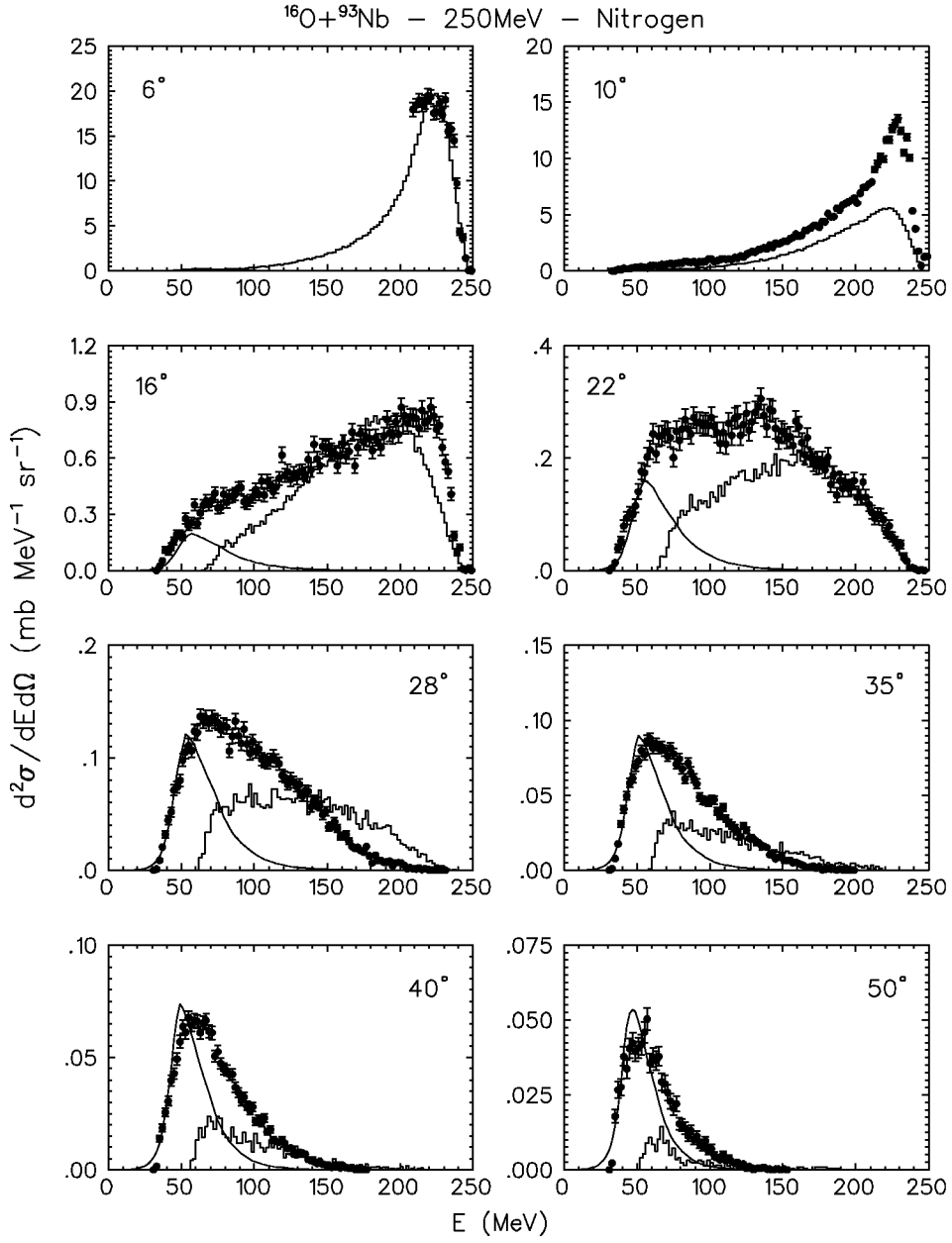

Fig. 13. Spectra of nitrogen fragments produced in the interaction of ^{16}O with ^{93}Nb at an incident energy of 250 MeV. The experimental cross-sections are given by the black circles, the theoretical predictions by the full lines (coalescence) and the histograms (break-up).

larger mass of ^{93}Nb which may thus be less perturbed in the fusion process. In the case of ^{197}Au we only measured the ^{8}Be spectra which do not extend down to the lowest possible energies due to the detection threshold of these fragments. This lack of information does not allow it to be ascertained whether in this case also one must assume that the nucleus from which the coalescence fragments are emitted is deformed.

The calculated coalescence spectra at 250 and 400 MeV (full lines in all relevant figures) reproduce accurately the observed spectra of the lowest-energy fragments. The values of the survival probability R_c have been found equal to 0.28 ± 0.03, 0.09 ± 0.03, 0.34 ± 0.05 and 0.15 ± 0.06 for, respectively ^{8}Be, boron, carbon [20] and nitrogen fragments with, possibly, a weak dependence on the target mass and the incident energy. The differences between these numerical values should not be taken too literally since they might be affected by the use of parameters whose values were fixed *a priori*. For instance, a slight variation of the values of the cluster Fermi energies could account for the observed differences in the R_c values which altogether are of the order of magnitude which we can expect. The case of $^{8}\mathrm{Be}_{gs}$ requires a little discussion. It is very unfortunate that in our experiment we could not measure their spectra below about 50 MeV. This threshold cuts most of the coalescence contribution.

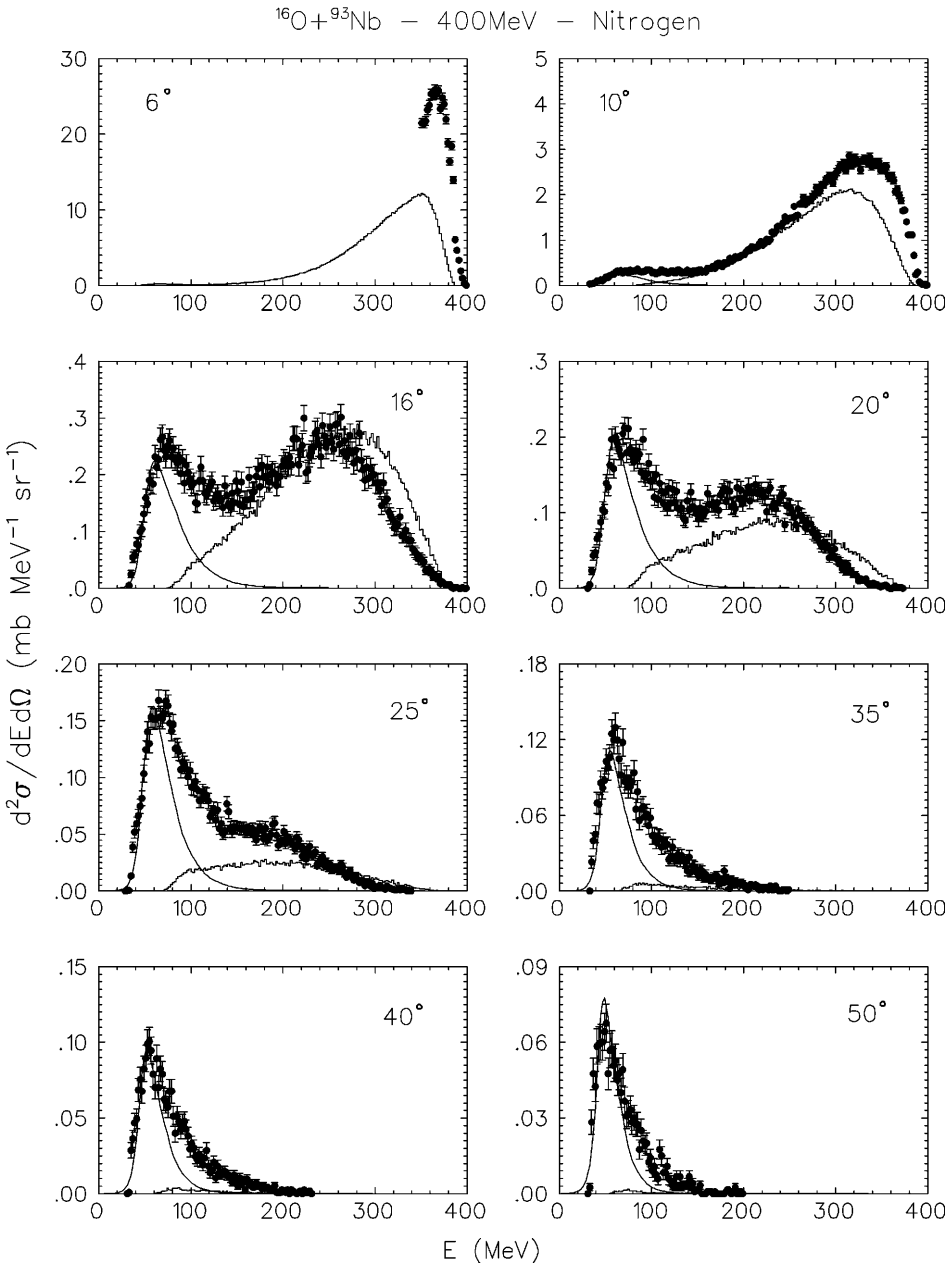

Fig. 14. Spectra of nitrogen fragments produced in the interaction of ^{16}O with ^{93}Nb at an incident energy of 400 MeV. The experimental cross-sections are given by the black circles, the theoretical predictions by the full lines (coalescence) and the histograms (break-up).

On the other hand it is quite clear, considering the comparison between measured and calculated spectra of ^{8}Be$_{gs}$ at angles larger than 12°, that the absolute value of the coalescence cross-section is estimated correctly using an R_c value of ≈ 0.28. This is very encouraging because this value is not significantly different from those of the other fragments, whose coalescence spectra are the sum of the contribution of many isotopes.

4 Conclusions

The spectra of the intermediate-mass fragments emitted in the interaction of ^{16}O with ^{59}Co and ^{93}Nb and in the case of ^{8}Be$_{gs}$ also with ^{197}Au are explained in this paper as due to the cumulative contribution of many single events in which a fragment is produced either by the break-up of the projectile or by the coalescence of nucleons. The latter mechanism proceeds during the cascade of N-N interactions by means of which the orderly kinetic energy of the nucleons of the composite nucleus created in the complete or partial fusion of the projectile and the target transforms into random thermal energy. For a fragment with charge and mass only slightly smaller than those of the projectile, the two reaction mechanisms are in most cases mutually exclusive. In fact, in the projectile's break-up this fragment is produced together with a complementary

Table 3. Cross-sections for complete fusion of oxygen and incomplete fusion of ^{12}C fragments which have been used for evaluating the coalescence spectra.

^{59}Co		
$E_{\rm inc}$ (MeV)	$\sigma_{\rm cf}$ (mb)	$\sigma_{\rm C}$ (mb)
250	590	500
400	369	670
^{93}Nb		
$E_{\rm inc}$ (MeV)	$\sigma_{\rm cf}$ (mb)	$\sigma_{\rm C}$ (mb)
250	732	320
400	452	580
^{197}Au		
$E_{\rm inc}$ (MeV)	$\sigma_{\rm cf}$ (mb)	$\sigma_{\rm C}$ (mb)
400	639	520

fragment with mass and charge considerably smaller and even if this fuses with the target nucleus, it is unlikely that in the subsequent thermalization process a fragment of charge and mass equal to those of the already produced heavy fragment will be formed. A fragment of charge and mass comparable to the projectile may be produced by nucleon coalescence only if the entire projectile or a considerable part of it fuses with the target nucleus, *i.e.* in a projectile's break-up in which a considerably lighter companion fragment is produced. The two reaction mechanisms are less exclusive if the fragments which are emitted have mass about one half of the projectile mass. However, our calculations suggest that, in this case also, these fragments are mostly produced by nucleon coalescence when the projectile or a fragment sizeably larger than the observed one, fuses with the target nucleus.

In both processes more than one isotope may contribute to the spectra of fragments of a given charge. However, the spread in mass of those which may be produced in the coalescence process is expected to be considerably larger, due to the statistical nature of the proposed mechanism. Unfortunately, this expectation could not be experimentally tested in this experiment. The fact that we reproduce with the same set of parameters and values of $R_{\rm c}$ of the same order of magnitude the coalescence contribution to the spectra of boron, carbon [20] and nitrogen (to which many isotopes contribute) and to the spectra of $^{8}{\rm Be}_{\rm gs}$ (where the contribution of only one fragment is to be considered) supports our interpretation. However, further experiments should be made to measure the isotope mass distributions whose reproduction constitutes a very significant test of any theoretical approach.

Finally, both processes develop during a very short time-scale. This is quite obvious in the case of break-up, but even nucleon coalescence, according to our calculations, takes less than about 5×10^{-22} s to occur after the time in which the two ions come into contact.

References

1. M. Blann *et al.*, Phys. Rev. C **44**, 431 (1991).
2. L.G. Moretto, Nucl. Phys. A **247**, 211 (1975).
3. M.S. Hussein, K.W. McVoy, D. Saloner, Phys. Lett. B **98**, 162 (1981).
4. B. Shivakumar *et al.*, Phys. Rev C **35**, 1730 (1987).
5. J. Aichelin *et al.*, Phys. Rev. C **37**, 2451 (1988).
6. D.H.E. Gross, Rep. Prog. Phys. **53**, 605 (1990).
7. L.G. Moretto, G.J. Wozniak, Annu. Rev. Nucl. Part. Sci. **43**, 379 (1993).
8. H. Fuchs, K. Möhring, Rep. Prog. Phys. **57**, 231 (1994).
9. C. Bhattacharya *et al.*, Phys. Rev. C **54**, 3099 (1996).
10. R. Neubauer *et al.*, Nucl. Phys. A **658**, 67 (1999).
11. Y. Larochelle *et al.*, Phys. Rev. C **62**, 051602-1 (2000).
12. H. Horiuchi, Nucl. Phys. A **685**, 260c (2001).
13. G. Poggi, Nucl. Phys. A **685**, 296c (2001).
14. G.R. Satchler, *Direct Nuclear Reactions* (Clarendon Press, Oxford, 1983).
15. E. Gadioli, P.E. Hodgson, *Pre-equilibrium Nuclear Reactions* (Clarendon Press, Oxford, 1992).
16. E. Gadioli *et al.*, Eur. Phys. J. A **8**, 373 (2000); **11**, 161 (2001).
17. S.L. Thomas, T. Davinson, A.C. Shotter, Nucl. Instrum. Methods A **288**, 212 (1990).
18. T. Davinson, A.C. Shotter, E.W. Macdonald, S.V. Springham, P. Jobanputra, A.J. Stephens, S.L. Thomas, Nucl. Instrum. Methods A **288**, 245 (1990).
19. E.W. Macdonald, A.C. Shotter, D. Branford, J. Rahighi, T. Davinson, N.J. Davis, Y. El Mohri, J. Yorkson, Nucl. Instrum. Methods A **317**, 498 (1992).
20. E. Gadioli *et al.*, Nucl. Phys. A **708**, 391 (2002).
21. K.W. McVoy, K. Nemes, Z. Phys. A **295**, 177 (1980).
22. I. Cervesato *et al.*, Phys. Rev. C **45**, 2369 (1992).
23. M. Cavinato *et al.*, Z. Phys. A **347**, 237 (1994).
24. J. Pouliot *et al.*, Phys. Rev. C **43**, 735 (1991).
25. R.R. Betts *et al.*, Phys. Rev. Lett. **39**, 1183 (1977).
26. M. Buenerd, *et al.*, Phys. Rev. Lett. **40**, 1482 (1978).
27. S. Landowne, A. Vitturi, *Inelastic scattering - nuclear*, in *Treatise on Heavy Ion Physics*, edited by D.A. Bromley, Vol. **I** (Plenum Press, New York and London, 1984) pp. 355-462.
28. R. Serber, Phys. Rev. **72**, 1008 (1947).
29. E. Gadioli *et al.*, Nucl. Phys. A **654**, 523 (1999).
30. E. Gadioli *et al.*, Phys. Lett. B **394**, 29 (1997).
31. E. Gadioli *et al.*, Nucl. Phys. A **641**, 271 (1998).
32. K.A. Korir *et al.*, in *Proceedings of the International Conference on Fundamental and Applied Aspects of Modern Physics, Luderitz, Namibia, 2000*, edited by S.H. Connell, R. Tegen (World Scientific, Singapore, 2001) pp. 535-542.
33. K. Siwek-Wylczyńska *et al.*, Phys. Rev. Lett. **42**, 1599 (1979).
34. K. Siwek-Wylczyńska *et al.*, Nucl. Phys. A **330**, 150 (1979).
35. A. Bonaccorso, J. Lhenry, T. Suomijarvi, Phys. Rev. C **49**, 329 (1994).
36. M. Cavinato *et al.*, Nucl. Phys. A **643**, 15 (1998).
37. M. Cavinato *et al.*, Nucl. Phys. A **679**, 753 (2001).
38. G.D. Harp, J.M. Miller, B.J. Berne, Phys. Rev. **165**, 1166 (1968).
39. M. Cavinato *et al.*, Phys. Rev. C **52**, 2577 (1995).
40. C. Brusati *et al.*, Z. Phys. A **353**, 57 (1995).
41. W.W. Wilcke *et al.*, At. Data Nucl. Data Tables **25**, 389 (1980).